Faculty of Science, Medicine and Health - Papers: part A

Faculty of Science, Medicine and Health

1-1-2014

Isomer-specific product detection of gas-phase xylyl radical rearrangement and decomposition using VUV synchrotron photoionization

Patrick Hemberger
Paul Scherrer Institute

Adam J. Trevitt
University of Wollongong, adamt@uow.edu.au

Thomas Gerber
Paul Scherrer Institute

Edward Ross
University of Melbourne

Gabriel da Silva
University of Melbourne, gdasilva@unimelb.edu.au

Recommended Citation

Isomer-specific product detection of gas-phase xylyl radical rearrangement and decomposition using VUV synchrotron photoionization

Abstract

Xylyl radicals are intermediates in combustion processes since their parent molecules, xylenes, are present as fuel additives. In this study we report on the photoelectron spectra of the three isomeric xylyl radicals and the subsequent decomposition reactions of the o-xylyl radical, generated in a tubular reactor and probed by mass selected threshold photoelectron spectroscopy and VUV synchrotron radiation. Franck-Condon simulations are applied to augment the assignment of elusive species. Below 1000 K, o-xylyl radicals decompose by hydrogen atom loss to form closed-shell o-xylylene, which equilibrates with benzocyclobutene. At higher temperatures relevant to combustion engines, o-xylylene generates styrene in a multistep rearrangement, whereas the p-xylylene isomer is thermally stable, a key point of difference in the combustion of these two isomeric fuels. Another striking result is that all three xylyl isomers can generate p-xylylene upon decomposition. In addition to C8H8 isomers, phenylacetylene and traces of benzocyclobutadiene are observed and identified as further reaction products of o-xylylene, while there is also some preliminary evidence for benzene and benzyne formation. The experimental results reported here are complemented by a comprehensive theoretical C8H8 potential energy surface, which together with the spectroscopic assignments can explain the complex high-temperature chemistry of o-xylyl radicals.

Keywords

GeoQuest

Disciplines

Medicine and Health Sciences | Social and Behavioral Sciences

Publication Details

Isomer-Specific Product Detection of Gas-Phase Xylyl Radical Rearrangement and Decomposition using VUV Synchrotron Photoionization

*Patrick Hemberger,[a] * Adam J. Trevitt,[b] T. Gerber,[a] Edward Ross, [c] Gabriel da Silva [c]*

a) Molecular Dynamics Group, Paul Scherrer Institute, 5232 Villigen PSI, Switzerland

b) School of Chemistry, University of Wollongong, New South Wales 2522, Australia

c) Department of Chemical and Biomolecular Engineering, The University of Melbourne, Victoria 3010, Australia

ABSTRACT:

Xylyl radicals are known intermediates in combustion processes since their parent molecules, xylenes, are present as fuel additives. In this study we report on the photoelectron spectra of the three isomeric xylyl radicals and the subsequent decomposition reactions of the *o*-xylyl radical, generated in a tubular reactor and probed by mass selected threshold photoelectron spectroscopy and VUV synchrotron radiation. Franck Condon simulations are applied to augment the assignment of elusive species. Below 1000 K, *o*-xylyl radicals decompose by hydrogen atom loss to form closed-shell *o*-xylylene, which equilibrates with benzocyclobutene. At higher temperatures relevant to combustion engines, *o*-xylylene generates styrene in a multi-step rearrangement, whereas the *p*-xylylene isomer is thermally stable, a key point of difference in the combustion of these two isomeric fuels. Another striking result is that all three xylyl isomers can generate *p*-xylylene upon decomposition. In addition to C_8H_8 isomers, phenylacetylene and traces of benzocyclobutadiene are observed and identified as further reaction products of *o*-xylylene, while there is also some preliminary evidence for benzene and benzyne formation. The experimental results reported here are complemented by a comprehensive theoretical C_8H_8 potential energy surface, which together with the spectroscopic assignments can explain the complex high-temperature chemistry of *o*-xylyl radicals.

1) Introduction

Aromatic hydrocarbons are widely used in fuels as additives due to their high energy densities and octane ratings. In order to reduce harmful benzene emissions, fuel compositions are now typically regulated to contain less than 1 %vol benzene, and from 2013 the US regulated the total amount to a maximum of 0.62 %vol.[1] In order to increase anti-knock properties of gasoline, whilst reducing benzene emissions, toluene and other polyalkylated benzenes (e.g. xylenes, trimethyl benzenes, ethylbenzene) are used instead. Since these species can form radicals more readily than benzene (sp^3 vs. sp^2 hybridized C-H bonds and the stability of corresponding radicals), and because the resultant benzylic radicals are generally unreactive towards O_2, an increased variety of side reactions can occur that may lead to the formation of polycyclic aromatic hydrocarbon (PAH) molecules, the precursors of soot. Experimental and theoretical investigations revealed that toluene pyrolysis leads mostly to the formation of benzyl radicals, which can decompose further by hydrogen atom loss to yield the five-membered ring fulvenallene (C_7H_6).[2-5] In 2009 it was found that a subsequent hydrogen abstraction could lead to fulvenallenyl radical (the global C_7H_5 minimum), which was unambiguously identified by measuring its mass-selected threshold photoelectron spectrum (ms-TPES).[6-8] The products arising from the dissociation of substituted benzyl radicals, however, are less well understood.
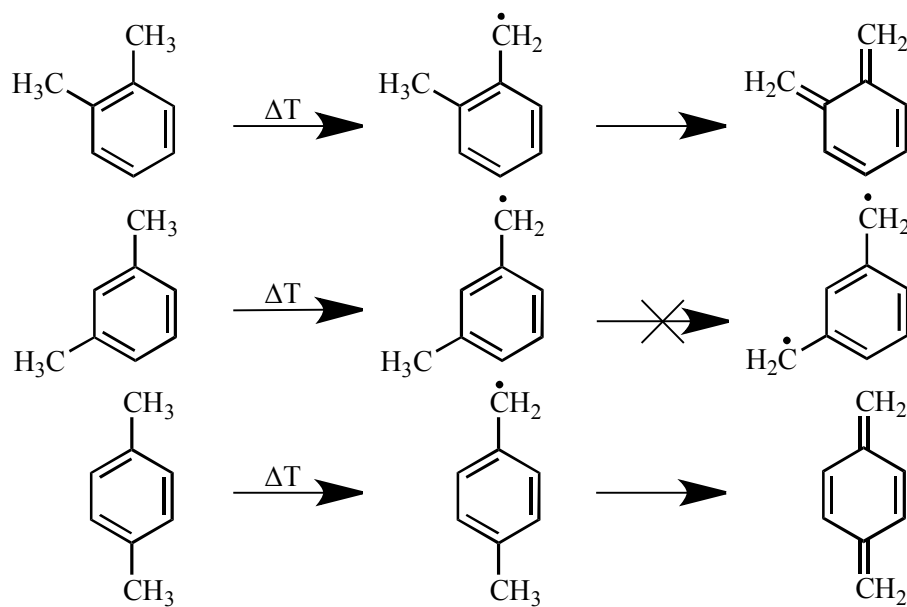
Scheme 1 Putative decomposition pathways of xylenes.

The decomposition dynamics of xylenes are also relatively unexplored, despite their prevalence in gasoline. It is generally accepted that the first xylene decomposition step is C-H bond fission at a methyl group yielding the corresponding xylyl (methylbenzyl) radical[9-10] (Scheme 1) but further unimolecular reactions have not been extensively studied. Possible decomposition products are the corresponding xylylenes, which appear after hydrogen abstraction (Scheme 1). While the *ortho* and the *para* isomers possess a closed shell character, *meta*-xylylene exists as a biradical, resulting in a structure that is 40-45 kcal/mol less stable than the *ortho* and *para* isomers.

In 1955 Farmer et al. investigated the three xylyl radicals by electron impact mass spectrometry (EI-MS) and their results suggested that the *meta* isomer does not decompose to form *m*-xylylene but rather one of the other two xylylene isomers.[11] In more recent times, a few studies have reported on xylene and xylyl radical decomposition. Shock tube experiments revealed that *o*- and *p*-xylyl radicals decompose faster than the *m*-xylyl radical and it was

assumed that the triplet *m*-xylylene does play an important role.[12] Farrell et al. observed a reduced burning velocity of *m*-xylyene compared to the *ortho* and *para* isomers and attributed this effect to the enhanced stability of *m*-xylyl radicals.[13] In 2009 it was predicted that *m*-xylyl preferably rearranges to *p*-xylyl and subsequently loses a hydrogen atom to yield *p*-xylylene via a maximum barrier of 70 kcal mol^{-1}, whereas the decomposition to *m*-xylylene and 3-methylfulvenallene must surmount 109 and 87 kcal mol^{-1} barriers, respectively.[10] Since the first study by Farmer et al. it took almost 60 years until this hypothesis could be proven spectroscopically,[14] with a recent study conclusively identifying *p*-xylylene as the dominant stable product of *m*-xylyl radical pyrolysis. Different from the *meta* case, the *ortho* and *para* xylyl radicals are widely assumed to decompose to their corresponding xylylenes, though this has not yet been demonstrated unequivocally. Moreover, there have been surprisingly few theoretical[15] and experimental[16,17] investigations carried out on the further rearrangement and decomposition processes of the xylylenes and other C_8H_8 isomers.

Using VUV photoionization techniques, coupled with a heated reactor source to selectively produce xylyl radical isomers, it is possible to intercept decomposition products by mass-selected threshold photoelectron spectroscopy (ms-TPES). We have shown that the imaging photoelectron photoion coincidence (iPEPICO) technique is a versatile tool for the online isomer-specific identification of reactive intermediates and their reaction products.[8, 18-19]

A few literature studies report VUV photoionization of xylyl radicals. The Farmer *et al*. study reported electron impact (EI) ionization potentials yielding values of 7.61, 7.65 and 7.46 eV for *ortho*, *meta* and *para* isomers respectively.[20] Later, photoelectron spectroscopy (PES) measurements carried out by Hayashibara and co-workers revised these values to 7.07, 7.12 and 6.96 eV, respectively.[21] The discrepancy between the EI study and the PES results was explained

by an underestimation of the onset of the ionization efficiency curve as measured with EI techniques. There was some evidence for vibrational structure present in the PES data, however assignments of these transitions were not carried out.

In this paper we report threshold photoelectron spectra of xylyl radicals and their decomposition products, which is vital for isomer-specific identification of these species in flames and other environments. Vibronic features are assigned with the aid of quantum chemical calculations and Franck-Condon (FC) simulations. Furthermore, we report a potential energy surface for rearrangement and dissociation of the C_8H_8 isomers to aid in our interpretation of the products formed upon *o*-xylyl radical pyrolysis.

2) Experimental and theoretical methods

The experiments were carried out at the VUV beamline at the Swiss Light Source (Paul Scherrer Institute), located in Villigen, Switzerland. The beamline and the iPEPICO endstation are only briefly described as a detailed description can be found in the literature.[22-24] The X04DB bending magnet provides the synchrotron radiation, which is collimated by a mirror onto a 600 mm^{-1} grating working in grazing incidence. A resolution of 5 meV (resolving power of around 1:3000) was achieved, measured by the 11s′ Rydberg series of argon. Higher grating orders are suppressed by a differentially pumped gas filter operating at 10 mbar with a mixture of argon (30 mol%), neon (60 mol%) and krypton (10 mol%). Below 7 eV an MgF_2 window was utilized. The iPEPICO endstation combines velocity map imaging (VMI) of the electrons with Wiley McLarren time-of-flight (TOF) mass spectrometry of ions. A constant field of 120 V/cm accelerates the charged particles onto a Jordan TOF (C-726) mass spectrometer and delay-line anode detector (Roentdek, DLD40) and the events are correlated in real-time in a multiple start –

multiple stop scheme.[25] Threshold electrons were selected with a resolution of 5 meV by selecting the central part of the image. The hot electron contamination was subtracted by the procedure outlined by Sztaray and Baer.[26] Subtracting the background in a TOF mass spectrum eliminates false coincidences. Chemical samples *o*-xylylbromide, *m*-xylylbromide and *p*-xylylbromide were commercially obtained from Sigma Aldrich and used without further purification. Infrared spectra of the precursors measured with a Bruker Vertex 70v spectrometer (see supporting information Figure S1) show no indication of isomer scrambling. A temperature-controlled bubbler containing the samples was heated between room temperature and 90 °C, to acquire sufficient vapor pressure. A seeding pressure of around 70 mbar argon was applied. The mixture was expanded through a 150 μm pinhole directly into a resistively heated SiC reactor, where the reactive intermediates are generated and the pyrolysis takes place. A molecular beam is formed and enters the spectrometer chamber without applying a skimmer, complicating the exact determination of flows, cooling, residence time and pressure in the reactor. The temperature was monitored in some experiments by measuring the surface temperature of the tubular reactor with a type C thermocouple. Due to variations in the quality of the thermocouple contact the accuracy of the temperature is only ± 100 K.[27] Note that the measured surface temperature is not necessarily the same as the gas temperature, and merely serves as an indicator of the thermal environment in the reactor which leads to changes in molecular composition.

Gaussian 09 was utilized for all quantum chemical calculations, applying the B3LYP functional and the 6-311++G(d,p) basis set to calculate equilibrium geometries.[28] These geometries and Hessian matrices were used to compute Franck-Condon factors with the program ezSpectrum.OSX,[29] which were subsequently convoluted with a Gaussian function for comparison with experiment. Reliable ionization energies and relative energies were calculated

using the G4[30] and CBS-QB3[31-32] methods. The C_8H_8 energy surface is developed using the composite G4 method. All reported electronic energies are corrected by the zero point energy.

3) Results

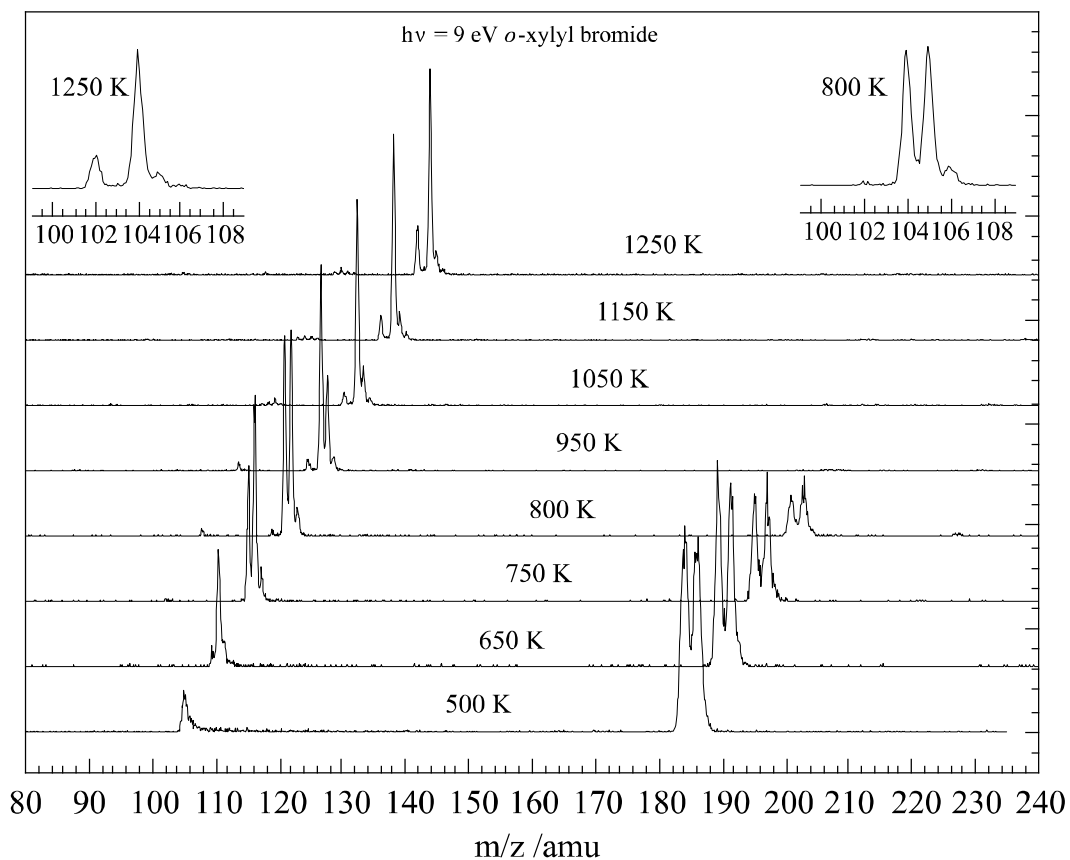### A) Generation and photoionization of the radicals

Figure 1   Mass spectra of *o*-xylyl bromide as a function of the reactor temperature at 9 eV photon energy. At lower temperatures only m/z = 105 is generated, which can be assigned to the *o*-xylyl radical. With increasing temperature the radical decomposes by H loss (m/z = 104), which further reacts to m/z = 102.

Mass spectra of *o*-xylyl bromide as a function of the pyrolysis temperature are depicted in **Figure 1**, showing that at as low as around 500 K (lowest trace) the fragment m/z = 105 is generated due to pyrolysis of the precursor according to Scheme 2:

CH_2Br

H_3C

$\xrightarrow[\text{-Br}]{\Delta T}$

$\overset{\bullet}{C}H_2$

H_3C
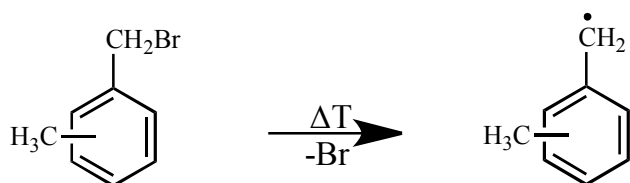
Scheme 2   Pyrolysis of brominated xylyl radical precursors.

With increasing temperature the *o*-xylyl bromide signal vanishes while the xylyl radical is detected. Starting at around 650 K (**Figure 1**) the radical then further decomposes by losing a hydrogen atom to form m/z = 104. At around 950 K, m/z = 104 is the most abundant peak in the mass spectrum. At similar temperatures another decomposition product appears at m/z = 102 and, as assigned below, most likely signifies a subsequent loss of H_2 from m/z 104. Minor species appearing in the mass spectra will be discussed later in this manuscript. A temperature breakdown diagram is depicted in Figure 2 showing the fractional abundance of the ion signal as a function of the temperature at fixed photon energy of 9 eV. Since absolute ionization cross-sections of the precursor are not available for all species, only the relative signals were taken into account in the plot that nevertheless yields a useful qualitative picture. At this photon energy the dissociative ionization of the precursor only plays a minor role.

At ~800 K the precursor, the *o*-xylyl radical and the m/z = 104 (C_8H_8) channel possess the same signal intensity. The C_8H_8 species undergo further reactions to form m/z = 102 (and

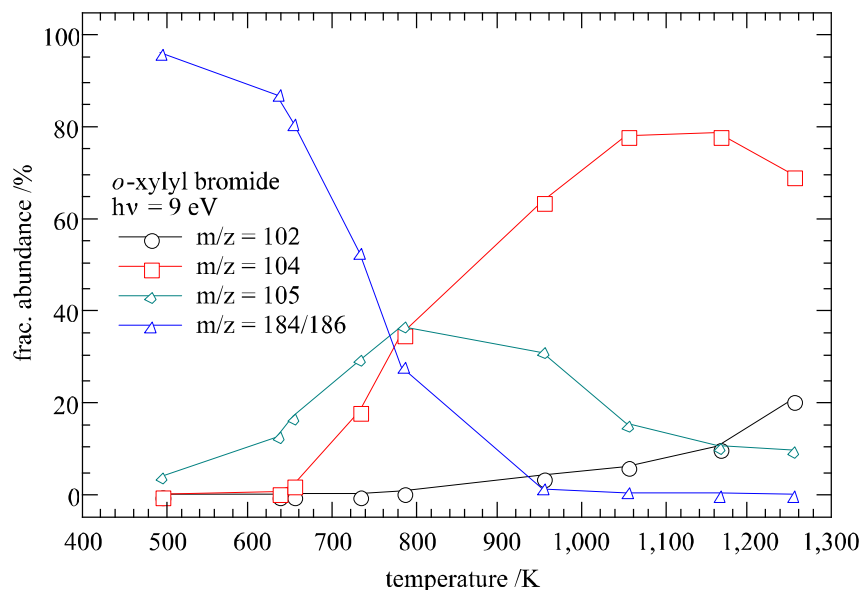possibly other undetected products that ionize at higher energies, *vide infra*) at around 800-1000 K.

Figure 2 Temperature breakdown diagram of *o*-xylyl bromide pyrolysis.

In order to elucidate the decomposition pathways of the three xylyl radicals, one has to ensure that each radical can be produced exclusively without the interference of the other isomers. Therefore, for each radical population that is generated by pyrolysis of its corresponding precursor (Scheme 2) a mass selected threshold photoelectron spectrum (ms-TPES) is recorded, which are depicted in Figure 3. It is immediately apparent that the three species have distinct ms-TPES. *o*-Xylyl radicals (Figure 3a) possess an adiabatic ionization energy (IE$_{ad}$) of 7.08 eV. Half the full width at half maximum (FWHM), 0.014 eV, of the 0-0 vibrational transition is reported as the experimental uncertainty. The TPES shows a vibrational progression with 0.061 eV spacing, corresponding to *ca.* 490 cm^{-1}. In order to further support this assignment Franck

Condon simulations were performed. Both the stick spectra and convolution with a FWHM of 28 meV are depicted in Figure 3a. The simulated spectra supports the assignment that the largest peak corresponds to the 0-0 transition, while the peak at 7.14 eV comprises two vibrational transitions, which are assigned as two in plane ($\nu_{28} = 503$ cm^{-1}, a$'$ and $\nu_{27} = 586$ cm^{-1}, a$'$) ring deformation modes. Both transitions possess totally symmetric character and are thus symmetry allowed.

The TPES of *m*-xylyl radical is shown in Figure 3b and exhibits what is likely a hot- or sequence-band transition at 7.05 eV, which corresponds to a vibrational frequency in the neutral of around 500 cm^{-1}. The IE$_{ad}$ can be assigned to the most intense transition at 7.11 ± 0.01 eV. A progression with 65 meV spacing dominates the TPES, which can be assigned according to a Franck-Condon simulation also depicted in Figure 3b.

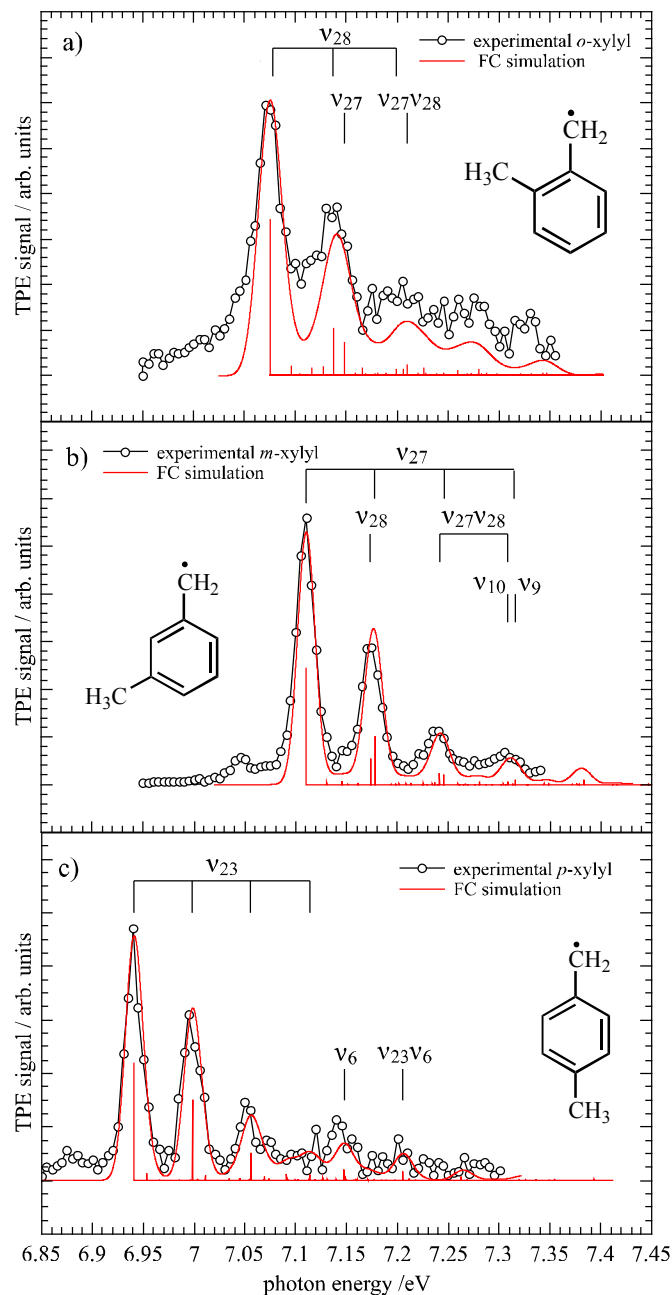**Figure 3** ms-TPE spectra of *ortho* (a), *meta* (b) and *para* (c) xylyl radicals. It is evident that the three radicals can be selectively generated and distinguished by their ionization energy and vibrational structure.

Two ring deformation modes ($\nu_{27} = 545$ cm^{-1}, a′ and $\nu_{28} = 509$ cm^{-1}, a′) mostly associated with C-C-C bending vibrations are active upon ionization of the *m*-xylyl radical. Both transitions

contribute to the peak at 7.18 eV. A combination band $^1 27^1 28$ and the first overtone of ν_{27} dominate the feature at 7.24 eV. Two C-C stretching vibrations $\nu_{10} = 1597$ cm^{-1} (a′) and $\nu_9 = 1657$ cm^{-1} (a′) contribute besides ν_{28} and ν_{27}, to the broad feature at 7.3 eV, as labeled in Figure 3b.

The ms-TPE spectrum and FC simulation of *p*-xylyl radicals are presented in Figure 3c. Apart from the small hot- or sequence-band transition at 6.88 eV the radical ionizes at 6.94 ± 0.01 eV adiabatically. A rich progression mostly due to activity in $\nu_{23} = 464$ cm^{-1} (a′), a C-C-C bending mode (ring moiety), dominates the spectrum after the origin. The fundamental of the ν_6 (1666 cm^{-1}, C-C stretch, a′) and the combination band with ν_{23} can be observed at 7.15 and 7.20 eV.

The adiabatic ionization energies obtained in this study are in excellent agreement with literature values of 7.07 ± 0.02 eV, 7.12 ± 0.02 eV and 6.96 ± 0.02 eV for *o*-, *m*-, and *p*-xylyl radicals respectively.[21] Higher resolution of the vibrational transition is afforded by the threshold photoelectron technique compared to the literature PE spectra.[21] According to DFT calculations the highest occupied molecular orbital (HOMO) of all the xylyl radicals are exclusively of π character, and are predominant about the CH$_2$ group and at position 2, 4 and 6 of the benzene moiety (relative to the radical site). In accord with Koopmans' theorem the electron is removed from the HOMO. Ions with a methyl group in the *ortho* and *para* positions should posses a larger stabilization since the positive charge can be efficiently stabilized by a CH$_3$ group due to hyperconjugation. The lower ionization energies of the *ortho* and *para* compared to the *meta* isomer can be attributed to this effect. Table 1 compares the experimental adiabatic IEs of the xylyl radicals with calculations and literature values. The electronic characters of these transitions are $X^+\ ^1a′ \leftarrow X\ ^2a''$ in the case of the *ortho* and *meta* xylyl radical, but $X^+\ ^1a′ \leftarrow X\ ^2a′$ in the unique case of the *para* isomer since the mirror plane is perpendicular to the molecular

plane. Orbitals of the xylyl radicals are provided in the supporting information (Figure S2). DFT calculations further reveal that a moderate change in geometry can be expected upon ionization of the radicals. The most pronounced structural change is the shortening of the $C\text{-}CH_2$ bond, which places some activity in C-C stretching modes in all of the three spectra. However the most pronounced vibrational transition is attributed to ring deformation-associated modes. Detailed computational data are given in the supporting information. In summary, the experimental TPE spectra reveal that the IE_{ad} and vibrational fingerprint can readily distinguish the radicals and each xylyl is generated cleanly in the pyrolysis reactor without rearrangement to one of the other isomers. Armed with this information, the further pyrolysis decomposition of these radical species is investigated.

Table 1   Summary of calculated, literature and experimental adiabatic ionization energies of the xylyl radicals

IE_{ad} / eV	Exp.	Lit.	B3LYP/ 6-311**G(d,p)	CBS-QB3	G4
o-xylyl	7.08	7.07	7.02	7.14	7.15
m-xylyl	7.11	7.12	7.06	7.16	7.18
p-xylyl	6.94	6.96	6.89	7.00	7.01

B. Identification of the *o*-xylyl decomposition products
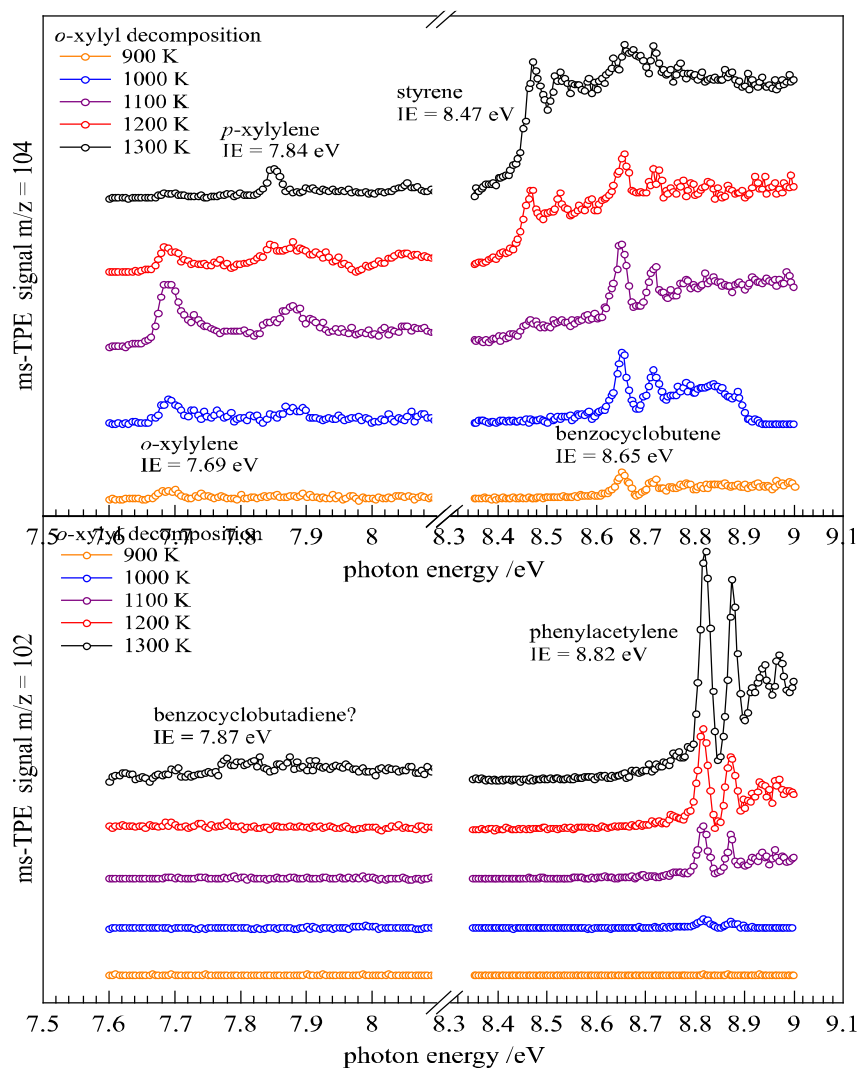
Figure 4   Reactor temperature dependent ms-TPES (m/z = 104, 102) arising from the decomposition of *o*-xylyl radicals. Four different isomers contribute to the mass channel m/z = 104. While at lower temperatures the spectrum is dominated by *o*-xylylene and benzocyclobutene, at higher pyrolysis temperatures *p*-xylylene and styrene are observed (a). Mass channel 102 shows a strong vibrational progression that can be assigned to phenylacetylene and minor contributions from benzocyclobutadiene (b).

15

The pyrolysis temperature was increased and ms-TPE spectra were acquired to probe the decomposition products with isomer specificity. Upon further heating a new signal at m/z = 104 appears and is consistent with the o-xylyl radical losing a hydrogen atom (see **Figure 1**). The corresponding ms-TPES of m/z = 104 is depicted in Figure 4 (upper part). Several features appear in a 7.6 – 8.8 eV energy range. At around 1000 K the broad peak at 7.69 eV can be assigned to the o-xylylene isomer. A conventional PES study by Kreile[33] et al., using 5,6-dimethylenebicyclo[2.2.1] hept-2-en-7-one as a precursor to pyrolytically generate o-xylylene, reported a vertical ionization energy of 7.7 eV for the ground state. Calculated ionization energies for this compound on the B3LYP/6-311++G(d,p) level of theory underestimated the IE by almost 500 meV (7.19 eV), whereas G4 and CBS-QB3 provide reliable values of 7.70 and 7.62 eV respectively. Upon ionization the molecular geometry is calculated to change from a non-planar structure – with the CH_2 groups bent above and below the ring plane – to a planar geometry for the cation; in addition both C-CH_2 bonds are elongated. The optimized geometries and force constants were used to calculate Franck-Condon factors and these are incorporated into simulated spectra that are depicted along with the measured spectra in Figure 5a.
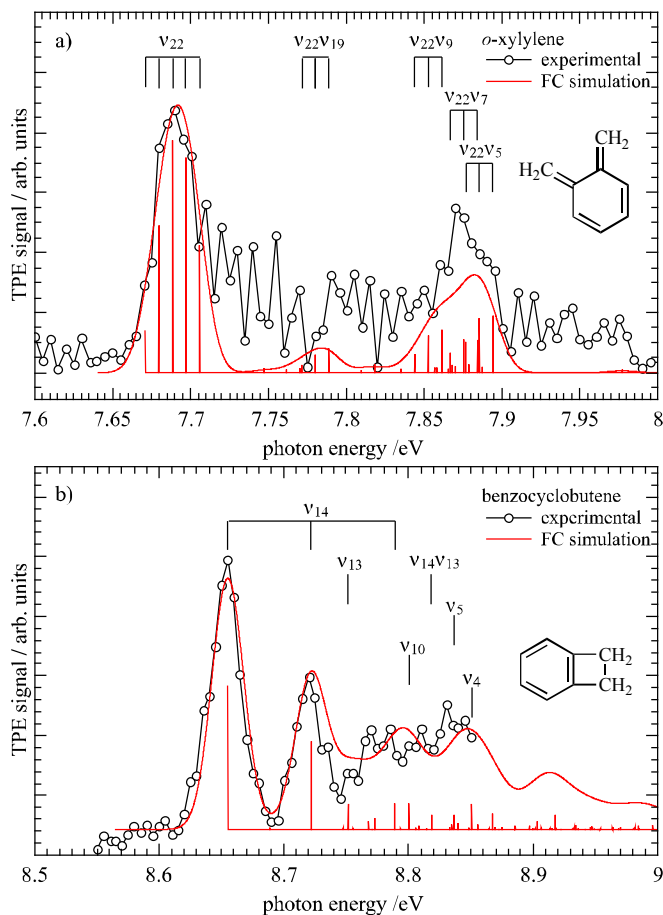
Figure 5   TPE spectra of mass channel m/z = 104 in the 7.6 - 8.9 eV energy range. The low energy part can be assigned to *o*-xylylene (a), whereas above 8.5 eV benzocyclobutene (b) is ionized. The red lines and sticks correspond to FC simulations and convolutions with Gaussian functions.

The simulation shows the first broad band at 7.69 eV consisting of several distinct transitions, which can be assigned to a progression of v_{22}, a CH_2 out-of-plane bending (a_2) vibration. The adiabatic ionization energy is difficult to assign due to the large change in geometry. According to the Franck-Condon simulation (red line) the 0-0 transition is located at 7.67 eV, we thus assign the IE_{ad} with a rather large uncertainty of 50 meV. Between 7.75 and 7.80 eV a combination transition between the out-of-plane bending mode of the ring ($v_{19} = 740$ cm^{-1}, a_2)

and ν_{22} is populated, as indicated in Figure 5a. The feature above 7.87 eV can be attributed to a collection of transitions: ν_9, ν_7 and ν_5 are in-plane C-CH$_2$ stretch and ring deformations (1325 cm^{-1}, a$_1$), CH$_2$ scissors, CH wagging motions (1509 cm^{-1}, a$_1$) and a combination between C-C stretches and CH$_2$ scissors (1589 cm^{-1}, a$_1$). All of them appear in combination with the ν_{22} vibration.

The mass-selected TPE spectrum at around 1000 K acquired between 8.55 eV and 9.00 eV for *m/z* 104 is depicted in Figure 5(b) shows a contribution that is assigned to benzocyclobutene, formed due to intramolecular [2+2] cycloaddition of *o*-xylylene. In the PES study of Kreile et al. benzocyclobutene was also observed at pyrolysis temperatures above 400 °C.[33]

Again, using quantum chemical calculations it is found that upon ionization the C-C bond of the 6-membered ring, where the C$_2$H$_4$ unit is located, expands by *ca.* 6 pm, which applies also for the C-C bond at the opposite side of the benzene ring. Additionally the C$_2$H$_4$ unit contracts by roughly 2 pm. Considering the HOMO of benzocyclobutene, electron density is removed from the benzene ring moiety, leading to a lowering of the bond order and thus to an elongation of these two bonds. This change in geometry influences the Franck Condon factors upon ionization, which are discussed as follows. The transition at 8.65 ± 0.015 eV is assigned to the IE$_{ad}$. Five active modes dominate the TPE spectrum in Figure 5(b). At 8.72 eV the fundamental of the CH-CH-C bending vibration is populated, having a computed frequency of 539 cm^{-1} (ν_{14}, a$_1$), which compares with an experimentally obtained value of around 560 cm^{-1}. Several transitions and their combination bands with the ν_{14} mode govern the range between 8.75 and 8.85 eV. Also assigned are ν_{13}, ν_{10}, ν_5 and ν_4 as mostly in-plane C-C stretch (ν_{13} = 779 cm^{-1}, a$_1$), C-H wagging (ν_{10} = 1173 cm^{-1}, a$_1$), anti-symmetric (ν_5 = 1462 cm^{-1}, a$_1$) and symmetric C-C stretching (ν_5 = 1578 cm^{-1}, a$_1$) vibrations, respectively, and are indicated in Figure 5(b).

Between 1100 and 1200 K the m/z = 104 ms-TPE spectrum (Figure 4(a) changes with new features at 7.84 and 8.47 eV appearing. The later one can be assigned to styrene according to its ionization energy of 8.46 eV (68 300 cm^{-1}) and vibrational fingerprint, a ring bending (ν_{28} = 470 cm^{-1}) motion.[34-36] In the low energy region of the spectrum, it is apparent that as the temperature is increased the o-xylylene signal decays and another peak at 7.84 eV clearly appears. We assign this peak to the p-xylylene C_8H_8 isomer. This is a particularly striking result – it does not matter which isomeric form of the radical is decomposed; all of them produce p-xylylene in appreciable amounts (see Figure 6). While the decomposition pathway of the p-xylyl radical to p-xylylene seems to be straightforward, since only a H loss channel is observed in the investigated temperature range, both the *meta* and the *ortho* radical isomers have to undergo complex intramolecular rearrangements to form p-xylylene. In a recent study we were able to prove experimentally that m-xylyl radicals rearrange to p-xylyl radicals, which subsequently decompose by H loss.[14] The rearrangement in the *ortho* case will be discussed *vide infra*. An IE$_{ad}$ of 7.85 eV can be determined for p-xylylene, in excellent agreement with the literature value of 7.87 eV.[37] Several vibrational transitions can be assigned according to a Franck-Condon simulation, shown in Figure 6. At around 7.9 eV the ν_8 C-C-C bending vibration is populated (473 cm^{-1}, a$_g$). The band between 8.00 and 8.05 eV consists of several transitions. In the shoulder to the lower energy side, transitions into the ν_6 (1213 cm^{-1}, a$_g$) and ν_5 (1380 cm^{-1}, a$_g$) are observed, corresponding to a CH wagging mode (ring moiety) and a C-C stretch of the CH$_2$ group. The ν_3 (1672 cm^{-1}, a$_g$) mode, a C-C stretching vibration of the ring carbon atoms, possesses the second highest Franck-Condon factors at 8.05 eV.
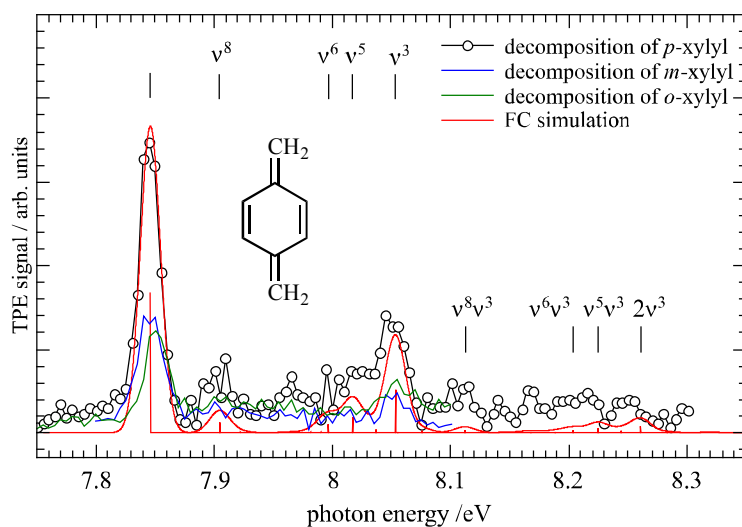
Figure 6 TPE spectrum and Franck-Condon simulation of *p*-xylylene. Green and blue curves correspond to spectra taken when *m*- and *p*-xylyl radicals were selectively prepared.

The part above 8.10 eV is governed by less intense transitions into combination bands and overtones. Figure 4(b) also shows the appearance of phenylacetylene, m/z = 102, which ionizes at 8.82 eV. According to the literature an ionization energy of 71 200 cm^{-1} (8.83 eV) was determined and a vibrational progression was assigned to a transition into the v_{13} = 460 cm^{-1} mode (6a$_1$), which is in excellent agreement with our findings and confirms that indeed phenylacetylene is formed upon decomposition.[36, 38-39] Since photoelectron spectra of both phenylacetylene and styrene are very well known and assigned, no further analysis of the transitions is performed. A summary of all species detected in the decomposition of *o*-xylyl radicals in this study is depicted in Scheme 3.
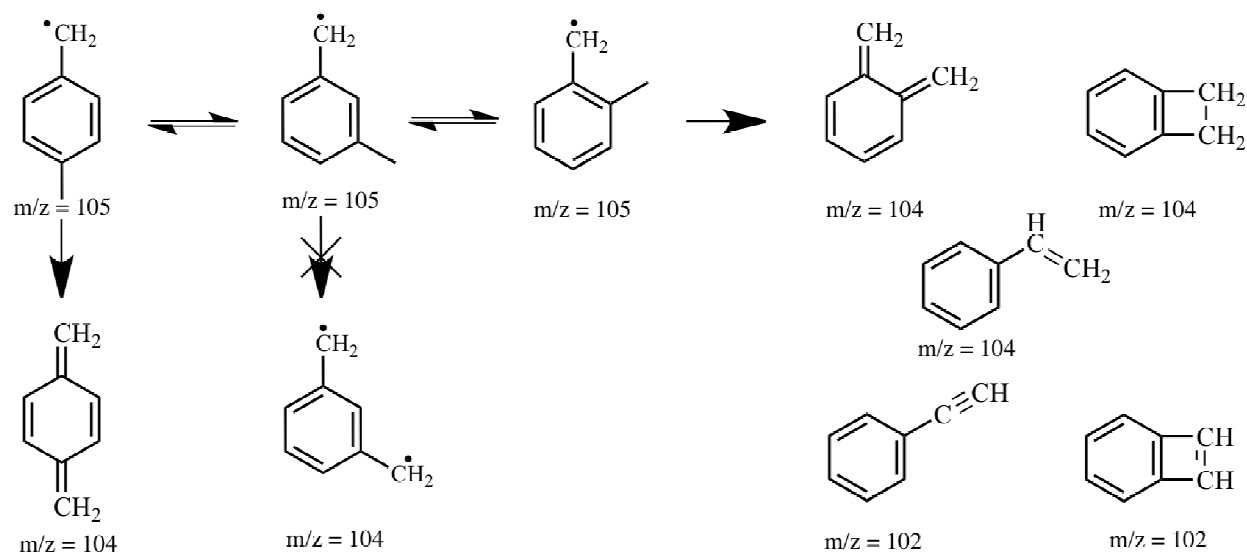
Scheme 3   Summary of the decomposition channels observed for the xylyl radicals.

4) Discussion: Implications for combustion chemistry

We have assigned up to four C_8H_8 (*m/z* 104) and two C_8H_6 (*m/z* 102) isomers appearing upon decomposition of *o*-xylyl radicals (*m/z* 105) at different temperatures using the iPEPICO technique. In the following we discuss reaction pathways that can potentially produce these products and their connection with combustion chemistry, augmented by high-level quantum chemical calculations. Of particular interest is the formation and decomposition of styrene, the global minima on the C_8H_8 surface. Styrene is reported to be formed in much greater quantities during the oxidation of *o*-xylene,[40] relative to the *meta* and *para* isomers.[41] This has been attributed to a direct pathway to styrene via the rearrangement of *o*-xylylene, and this process is thought to contribute to the different combustion properties of the isomeric xylene fuel molecules. It is therefore critical that we understand *o*-xylylene formation from xylyl radical pyrolysis, as well as the isomerization and decomposition pathways available to both *o*-xylylene and styrene.
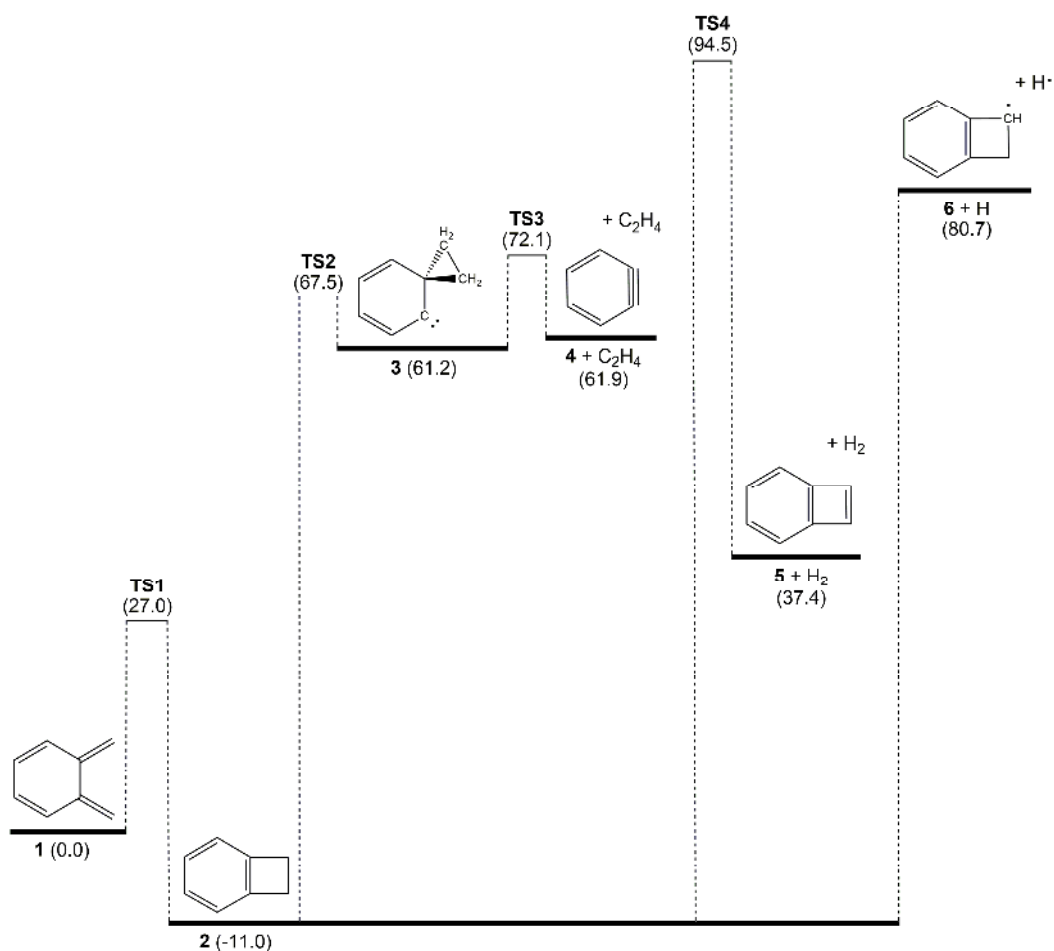
Figure 7 Energy diagram for *o*-xylylene (**1**) decomposition to benzyne (**4**) + ethene, cyclobutadiene (**5**) + H_2, and the C_8H_7 radical **6** + H. Energies are 0 K enthalpies relative to *o*-xylylene, in kcal/mol, calculated at the G4 level of theory.

Presented here are energy diagrams corresponding to the formation of salient C_8H_8 isomers and decomposition products in the isomerization and decomposition of *o*-xylylene. In all instances, energies were calculated using the G4 theoretical method. Details of the mechanism of these C_8H_8 rearrangements, as well as kinetic simulations for important isomerization and decomposition reactions, will be described in detail in a forthcoming companion paper.

At intermediate temperatures (900 – 1000 K) the *o*-xylyl radical decomposes by hydrogen loss to yield two C_8H_8 isomers, which were identified (Figure 4 & Figure 5) as *o*-xylylene and benzocyclobutene. This observation can be understood as follows. After generation of the *o*-xylyl radical it readily yields *o*-xylylene by C-H bond fission with a barrier of 69.6 kcal/mol.[14] Since a broad thermal energy distribution exists in pyrolysis experiments, a proportion of the *o*-xylylene population possesses enough internal energy to subsequently overcome a barrier of 27 kcal/mol to form benzocyclobutene (see Figure 7). The latter species is more stable than *o*-xylylene by 11 kcal/mol presumably indicating that the gained aromaticity outweighs the added ring strain. Since the reverse barrier to reform *o*-xylylene is also rather modest (38 kcal/mol) both species are formed at equilibrium below around 1100 K. If the temperature is increased to 1200 K, *o*-xylylene can further isomerize to form styrene. A barrier of 57.8 kcal/mol (**TS5 –** Figure 8) initiates the reaction to form a carbene intermediate (**7**), which presents the highest barrier for this process (see Figure 8). Subsequent ring closure to a three-membered ring, ring expansion to methyl cycloheptatetraene and again three membered ring formation and opening leads to methyl phenylcarbene, which undergoes a 1,2-hydrogen shift to yield styrene (**12**). This mechanism is in concord with the findings of Chapman et al.[16-17] and the proposal of Emdee *et al.*[40] that *o*-xylylene isomerization to styrene can take place during *o*-xylene combustion.
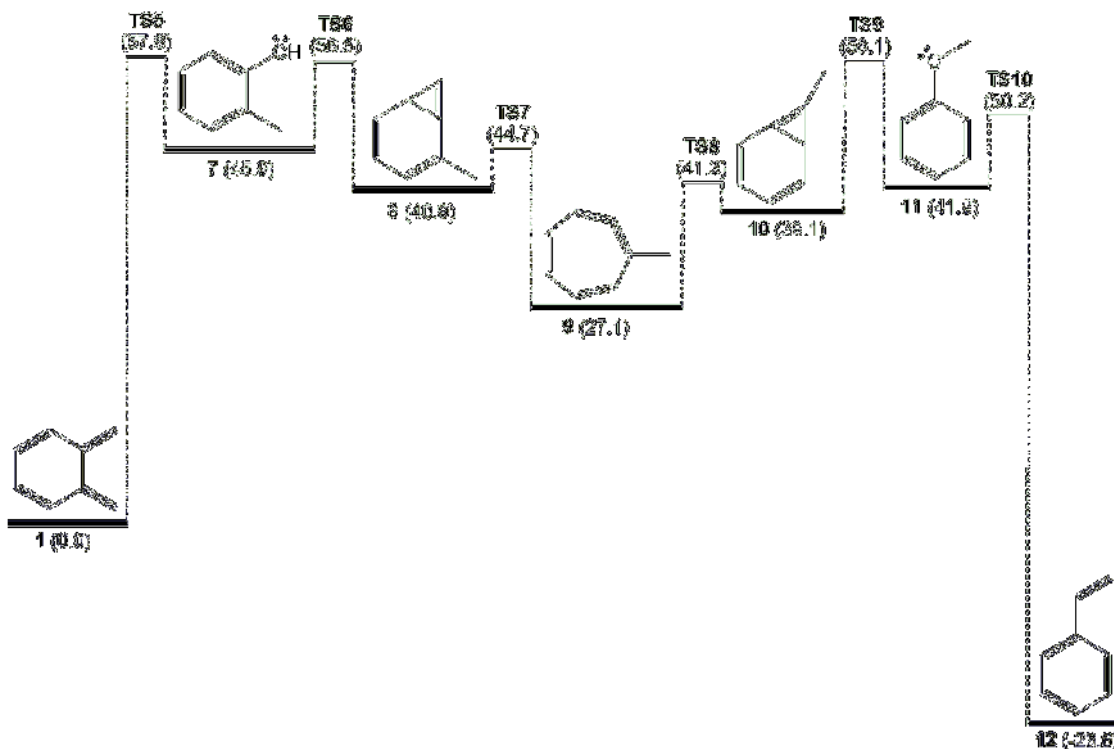
Figure 8 Energy diagram for *o*-xylylene (**1**) isomerisation to styrene (**12**). Energies are 0 K enthalpies relative to *o*-xylylene, in kcal/mol, calculated at the G4 level of theory.

Once styrene is formed, we identify four energetically competitive routes for its further decomposition. Styrene can initially undergo a 1,2 hydrogen shift to form the carbene **13**, overcoming a 79.1 kcal/mol energy barrier with respect to styrene (see Figure 9). Subsequently **13** can undergo a series of isomerisation steps, culminating in the formation of benzene plus vinylidene (CCH_2), a carbene isomer of acetylene. The reactive carbene moiety in **13** forms two bonds in a concerted process to provide the tricyclic structure **14**. A ring opening process then takes place to produce a seven membered ring, resulting in the formation of **15**. A succession of ring destruction and formation processes then follow (**16** - **17**), whereby the original six membered ring structure is recovered. **17** can then dissociate to form benzene via the direct loss of vinylidene, resulting in the destruction of the three-membered ring and thus restoring

24

aromaticity to the nascent benzene moiety. This last step also corresponds to the highest barrier along this pathway, with the corresponding transition state **TS16** being 84.8 kcal/mol above styrene. On the other hand, styrene can also directly dissociate to form benzene plus vinylidene (**TS17**), however this is anticipated to only be a minor channel, since this process has a barrier height of 94.6 kcal/mol, over 10 kcal/mol larger than the multi-step process.
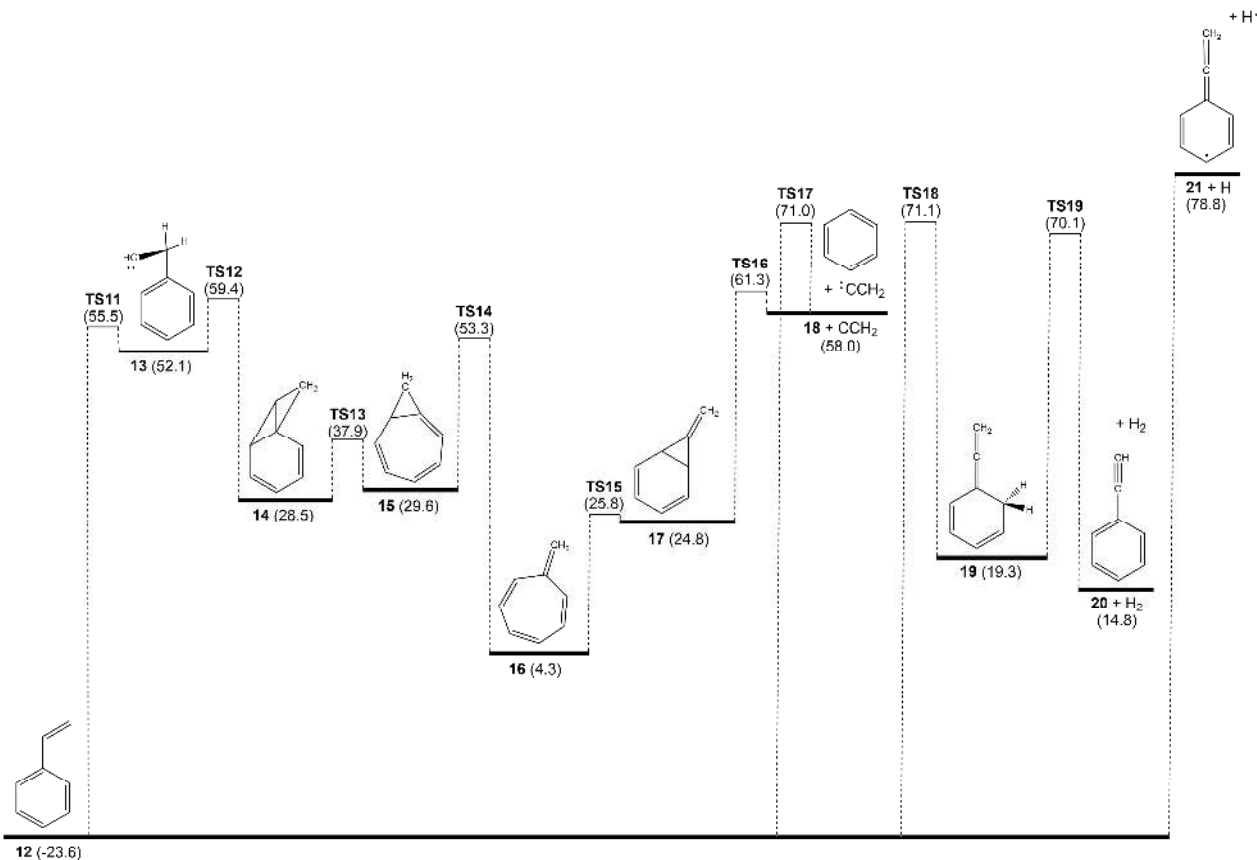
Figure 9   Energy diagram for styrene (**12**) decomposition to benzene (**18**) + vinylidene (CCH$_2$), phenylacetylene (**20**) + H$_2$ and the C$_8$H$_7$ radical **21** + H. Energies are 0 K enthalpies relative to *o*-xylylene, in kcal/mol, calculated at the G4 level of theory

Although this represents the first exposition of the dominant styrene decomposition mechanism, our finding that vinylidene (not acetylene) is the direct pyrolysis product of styrene is consistent with the previous assertion of Grela et al.[42] Note however that the almost negligible

25

barrier for isomerisation of vinylidene to acetylene (only a few kcal/mol)[43] means that vinylidene will promptly rearrange to yield acetylene in our experiments as well as when produced in flames. The calculated barrier height for decomposition of styrene of around 80 kcal/mol is also commensurate with previously reported experimental activation energies for this process.[42, 44]

Comparing the overall barrier height for styrene decomposition relative to the originating molecule *o*-xylylene (61.3 kcal/mol) we find that it is only marginally above that for the initial rearrangement of *o*-xylylene to styrene (57.8 kcal/mol), and some direct (chemically activated) dissociation of *o*-xylylene to yield benzene is expected at the low pressures encountered in these experiments. The direct formation of benzene from *o*-xylylene produced in *o*-xylene oxidation, in addition to styrene, may need to be considered in combustion models. It is also of interest to note that the overall barrier height for *o*-xylylene decomposition is similar to that for the isoelectronic molecule *o*-quinone methide,[45-47] despite the latter process being considerably less endothermic due to the formation of CO vs. CCH_2.

Another decomposition channel to be discussed is the loss of a hydrogen molecule to yield phenylacetylene (**20**) (m/z = 102). In a two-step process, styrene (see Figure 9) can undergo a H shift to an *ortho* site on the benzene ring (**TS18**, 94.7 kcal/mol, relative to styrene), resulting in an allenic structure. A six membered transition state (**TS19,** 93.6 kcal/mol, relative to styrene) corresponding to the simultaneous removal of a H atom from the *ortho* site on the benzene ring and the *β*-carbon on the allenic side-chain allows for the expulsion of a hydrogen molecule to yield phenylacetylene. Furthermore, styrene can lose a hydrogen atom to form the resonantly stabilized C_8H_7 radical **21**. This requires a barrier of 102.4 kcal/mol to be overcome. This C_8H_7 species can then lose another hydrogen to form phenylacetylene with barrier of only 41.2 kcal mol^{-1}; under the temperatures encountered in the experiments reported here this C_8H_7 radical will

rapidly decompose, providing an additional source of phenylacetylene. Seeing as bimolecular reactions between styrene and available free radicals (likely H atoms) within the flow reactor will also yield this same C_8H_7 isomer, this provides yet another pathway to the observed product phenylacetylene.

While we have shown that *o*-xylylene can decompose to a variety of different species after first isomerising to styrene, a couple of other high temperature dissociation pathways are also accessible via benzocyclobutene. The four-membered ring on benzocyclobutene can rearrange to yield a three-membered ring structure to produce the carbene isomer 3 (see Figure 7). This is then followed by subsequent C_2H_4 loss to form benzyne (**4**). The latter step has the highest barrier to overcome, at 72.1 kcal/mol with respect to *o*-xylylene. Although we are unaware of any previous studies that have considered benzyne as a C_8H_8 decomposition product, the reverse process has been investigated before using both experimental and theoretical methods.[48,49]

Benzocyclobutene can also lose a H atom on the four-membered ring to form another C_8H_7 radical (**6**) after surmounting a barrier of 80.7 kcal/mol relative to *o*-xylylene. This species can then lose a further H atom to form benzocyclobutadiene (with barrier of 60.7 kcal mol^{-1}), thus providing a possible explanation for the presence of benzocyclobutadiene in the experiments. In this case, given the high energy required for C-H bond homolysis in the parent, bimolecular chemistry first leading to the C_8H_7 species is likely to be the dominant originator of the small quantities of benzocyclobutadiene observed. Also note that it is possible to directly eliminate H_2 in benzocyclobutene to form benzocyclobutadiene (**TS4** in Figure 7), but the barrier is too high to compete with the other identified reaction channels.

The observation of *p*-xylylene is somewhat puzzling if *o*-xylyl is the decomposing radical. We would like to note that Figure 6 shows the appearance of *p*-xylylene independent of which

isomeric form of the radical decomposed. Our recent work can explain this observation of *p*-xylylene at around 1300 K.[14] *m*-Xylyl radicals do not appear to decompose to form *m*-xylylene diradicals,[50-52] since a thermodynamically more stable pathway is accessible.[14] This reaction channel describes the rearrangement of the *meta* radicals over bicyclic intermediates followed by rate-determining ring-opening/ring-closing sequences, with subsequent hydrogen loss. A similar mechanism can be applied starting with *o*-xylyl radicals, where these radicals undergo a rearrangement process to *m*- then *p*-xylyl radicals, which subsequently decompose to the detected *p*-xylylene. The reason that this reaction channel is not observed at lower temperatures is purely due to kinetic considerations. While at lower temperatures the rearrangement to form *p*-xylyl is slow, this reaction will be more rapid at higher bath gas temperatures and significant branching between either H loss to form *o*-xylylene or the rearrangement to *p*-xylyl radicals can occur. The latter radical subsequently decomposes by H loss. The thermal decomposition of the less-stable *o*-xylylene isomer at higher temperatures will also increase the relative signal intensity of thermally stable *p*-xylylene.
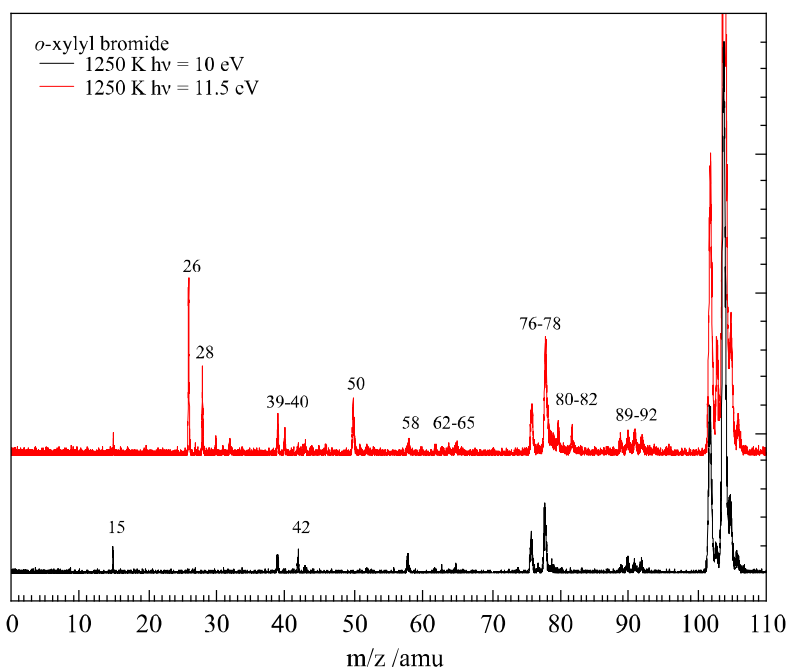
Figure 10   Mass spectra of *o*-xylyl bromide at 1250 K measured at 10 and 11.5 eV photon energy.

Although the above analysis can explain all of the observed C_8H_8 and C_8H_6 products originating from *o*-xylyl radical pyrolysis, it also suggests a number of other important decomposition products for which ms-TPES were unavailable. Here we would like to discuss the appearance of these lighter fragments ionizing at higher photon energies. Figure 10 shows two mass spectra taken at 10.0 and 11.5 eV photon energy and a reactor temperature of 1250 K. Some impurities should be mentioned first. Mass spectra without pyrolysis show traces of benzylbromide (*m/z* = 170, 172), which can react to form benzyl radicals, fulvenallene, fulvenallenyl and toluene and can explain the peaks between *m/z* = 89 and 92. In previous experiments acetone (*m/z* = 58) has been used as a mass calibrant, delivering ketene (*m/z* = 42) and methyl radicals (*m/z* = 15) upon pyrolysis. The appearance of *o*-benzyne (*m/z* = 76) and ethene (*m/z* = 28) is consistent with the thermal

29

decomposition of *o*-xylylene via the mechanism presented in Figure 7. The appearance of acetylene ($m/z = 26$) and benzene ($m/z = 78$) can be explained by unimolecular dissociation of styrene (Figure 9). According to the literature both the benzyne and benzene products cannot be formed by benzyl, fulvenallene or fulvenallenyl decomposition reactions, since this would involve C, CH or CH_2 bond rupture.[53] Recombination of two propargyl radicals ($m/z = 39$) to benzene or fulvene only plays a subordinate role, since other bimolecular reaction products like HBr ($m/z = 80/82$) and xylenes ($m/z = 106$) can be observed only in small amounts in the mass spectra. Taking into account the relative cross-sections at 10 eV of benzene and propargyl, the signal intensity can be approximated as the ratio 1:4 propargyl to benzene.[54-55] If the recombination was playing a large role one would expect a reversed relative abundance. C_4H_2, diacetylene, and acetylene are reaction products of *o*-benzyne ($m/z = 76$) decomposition, which is also present in the mass spectrum at 11.5 eV (see Figure 10).[56]

The propargyl radical could have several origins. Benzyl radicals can decompose to form fulvenallenyl radicals, which can subsequently dissociate to yield diacetylene ($m/z = 50$, C_4H_2) and propargyl radicals.[48] However, in the fulvenallenyl measurements[48] it seemed that at a higher temperature the ratio between $m/z = 89$ and $m/z = 39$ was very similar, whereas in the mass spectra of Figure 10 the propargyl is the dominating peak, which suggests that the contribution of $m/z = 89$ to 39 is only of minor importance. Consequently most of the propargyl is thought to result from decomposition of other species, including C_8H_n and C_6H_n compounds.

5) Conclusion

In this study the threshold photoionization of combustion relevant xylyl (methylbenzyl) radicals were investigated. We were able to show that *ortho*, *meta* and *para* isomers can be

synthesized in a pyrolysis reactor in an isomer-specific manner. In order to verify this, we performed Franck-Condon simulations and were able to assign the peaks in the ms-TPES to their vibrational transitions. The adiabatic ionization potentials were determined to be 7.08 ± 0.02 eV, 7.11 ± 0.02 eV and 6.94 ± 0.02 eV for o-, m-, and p-xylyl radicals respectively in excellent agreement with literature values and quantum chemical calculations.

By increasing the pyrolysis temperature the o-xylyl radical decomposes by hydrogen atom loss to yield o-xylylene and benzocyclobutene at lower temperatures. At higher temperatures the latter compound vanished from the ms-TPE spectrum and p-xylylene and styrene are generated instead. Another decomposition channel (C_8H_6) can also be observed starting at intermediate reactor temperatures and can be assigned to phenylacetylene and minor contributions of benzocyclobutadiene. The assignments were supported by literature threshold ionization spectra or by performing Franck-Condon simulations and high-level quantum chemical calculations.

Each xylyl radical isomer decomposes by H loss to yield p-xylylene. This is obvious as far as the p-xylyl radical is concerned, since simple hydrogen abstraction takes place from the remaining CH_3 group. Direct C-H bond fission in the case of m-xylyl would result in the triplet m-xylylene, a diradical, which is not observed. In a recent study we found that indeed a rearrangement to p-xylyl radicals occur upon pyrolysis, which further decompose by H atom loss.[14] We propose that a fraction of o-xylyl radicals that do not follow its dissociation to o-xylylene, undergoes a similar rearrangement, ultimately yielding p-xylylene.

We were able to identify four distinct C_8H_8 isomers as the decomposition products of o-xylyl radicals, by means of reactor temperature dependent ms-TPE spectra. Furthermore, another two C_8H_6 isomers could be observed, namely phenylacetylene and smaller contributions of benzocyclobutadiene, enabling us to map the potential energy surface of gas phase o-xylyl

radicals. Benzene, benzyne, acetylene and ethylene were also identified as further decomposition products of the *o*-xylyl radical.

To complement the experimental work performed and discussed in this paper, a comprehensive C_8H_8 energy surface was also developed for *o*-xylylene isomerisation and decomposition. Five distinct dissociation products were determined, of which three are accessible via styrene and two are accessible via benzocyclobutene. The mechanism was shown to account for many of the products observed in the experiments, and serves to demonstrate the complex chemistry that takes place during *o*-xylyl pyrolysis

ASSOCIATED CONTENT

Supporting Information. Infrared spectra of the precursors, HOMOs of the xylyl radicals and details on the molecular structures of neutrals and ions. This information is available free of charge via the Internet at http://pubs.acs.org

AUTHOR INFORMATION

Corresponding Author

*Patrick Hemberger. * patrick.hemberger@psi.ch

References

(1)   Agency, E. U. S. E. P. *Summary and Analysis of the 2009 Gasoline Benzene Pre-Compliance Reports*; 2009.

(2)   Cavallotti, C.; Derudi, M.; Rota, R. On the Mechanism of Decomposition of the Benzyl Radical. *Proc. Comb. Inst.* **2009,** *32*, 115-121.

(3)   da Silva, G.; Cole, J. A.; Bozzelli, J. W. Thermal Decomposition of the Benzyl Radical to Fulvenallene (C_7H_6) + H. *J. Phys. Chem. A* **2009,** *113*, 6111-6120.

(4)   Li, Y.; Zhang, L.; Tian, Z.; Yuan, T.; Wang, J.; Yang, B.; Qi, F. Experimental Study of a Fuel-Rich Premixed Toluene Flame at Low Pressure. *Energy Fuels* **2009,** *23*, 1473-1485.

(5)   Hansen, N.; Kasper, T.; Klippenstein, S. J.; Westmoreland, P. R.; Law, M. E.; Taatjes, C. A.; Kohse-Höinghaus, K.; Wang, J.; Cool, T. A. Initial Steps of Aromatic Ring Formation in a Laminar Premixed Fuel-Rich Cyclopentene Flame. *J. Phys. Chem. A* **2007,** *111*, 4081-4092.

(6)   da Silva, G.; Bozzelli, J. W. The C_7H_5 Fulvenallenyl Radical as a Combustion Intermediate: Potential New Pathways to Two- and Three-Ring PAHs. *J. Phys. Chem. A* **2009,** *113*, 12045-12048.

(7)   Zhang, T.; Zhang, L.; Hong, X.; Zhang, K.; Qi, F.; Law, C. K.; Ye, T.; Zhao, P.; Chen, Y. An Experimental and Theoretical Study of Toluene Pyrolysis with Tunable Synchrotron VUV Photoionization and Molecular-Beam Mass Spectrometry. *Comb. Flame* **2009,** *156*, 2071-2083.

(8)   Steinbauer, M.; Hemberger, P.; Fischer, I.; Bodi, A. Photoionization of C_7H_6 and C_7H_5: Observation of the Fulvenallenyl Radical. *ChemPhysChem* **2011,** *12*, 1795-1797.

(9)   Da Costa, I.; Eng, R. A.; Gebert, A.; Hippler, H. Direct Observation of the Rate of H-Atom Formation in the Thermal Decomposition of Ortho-, Meta-, and Para-Xylene behind Shock Waves between 1300 and 1800 K. *Proc. Comb. Inst.* **2000,** *28*, 1537-1543.

(10)   da Silva, G.; Moore, E. E.; Bozzelli, J. W. Decomposition of Methylbenzyl Radicals in the Pyrolysis and Oxidation of Xylenes. *J. Phys. Chem. A* **2009,** *113*, 10264-10278.

(11)   Farmer, J. B.; Marsden, D. G. H.; Lossing, F. P. Thermal Stability of Ortho-, Para-, and Meta-Xylyl Radicals and the Formation of Quinodimethanes. *J. Chem. Phys.* **1955,** *23*, 403-404.

(12)   Fernandes, R. X.; Gebert, A.; Hippler, H. The Pyrolysis of 2-, 3-, and 4-Methylbenzyl Radicals behind Shock Waves. *Proc. Comb. Inst.* **2002,** *29*, 1337-1343.

(13)   Farrell, J.; Johnston, R.; Androulakis, I. Molecular Structure Effects On Laminar Burning Velocities At Elevated Temperature And Pressure. *SAE Paper* **2004,** *2004-01-2936.*

(14)   Hemberger, P.; Trevitt, A. J.; Ross, E.; da Silva, G. Direct Observation of para-Xylylene as the Decomposition Product of the meta-Xylyl Radical Using VUV Synchrotron Radiation. *J. Phys. Chem. Lett.* **2013,** *4*, 2546-2550.

(15)   Garifzianova, G.; Khrapkovskii, G. Theoretical Study of the Potential Energy Surface for CH_3 and CH_4 losses from Ethyltoluenes. *Theor. Chem. Acc.* **2009,** *124*, 439-444.

(16)   Chapman, O. L.; Tsou, U. P. E.; Johnson, J. W. Thermal Isomerization of Benzocyclobutene. *J. Am. Chem. Soc.* **1987,** *109*, 553-559.

(17)   Chapman, O. L.; Johnson, J. W.; McMahon, R. J.; West, P. R. Rearrangements of the Isomeric Tolylmethylenes. *J. Am. Chem. Soc.* **1988,** *110*, 501-509.

(18)   Lang, M.; Holzmeier, F.; Fischer, I.; Hemberger, P. Threshold Photoionization of Fluorenyl, Benzhydryl, Diphenylmethylene, and Their Dimers. *J. Phys. Chem. A* **2013,** *117*, 5260-5268.

(19)   Holzmeier, F.; Lang, M.; Hader, K.; Hemberger, P.; Fischer, I. H_2CN^+ and H_2CNH^+: New insight into the Structure and Dynamics from Mass-Selected Threshold Photoelectron Spectra. *J. Chem. Phys.* **2013,** *138*, 214310.

(20)   Farmer, J. B.; Lossing, F. P.; Marsden, D. G. H.; McDowell, C. A. Free Radicals by Mass Spectrometry. VIII. The Ionization Potentials of Para-, Ortho-, and Meta-Xylyl Radicals. *J. Chem. Phys.* **1956,** *24*, 52-55.

(21)   Hayashibara, K.; Kruppa, G. H.; Beauchamp, J. L. Photoelectron Spectroscopy of the o-, m-, and p-Methylbenzyl Radicals. Implications for the Thermochemistry of the Radicals and Ions. *J. Am. Chem. Soc.* **1986,** *108*, 5441-5443.

(22)   Bodi, A.; Hemberger, P.; Gerber, T.; Sztaray, B. A New Double Imaging Velocity Focusing Coincidence Experiment: i2PEPICO. *Rev. Sci. Instrum.* **2012,** *83*, 083105-8.

(23)   Bodi, A.; Johnson, M.; Gerber, T.; Gengeliczki, Z.; Sztaray, B.; Baer, T. Imaging Photoelectron Photoion Coincidence Spectroscopy with Velocity Focusing Electron Optics. *Rev. Sci. Instrum.* **2009,** *80*, 034101-7.

(24)   Johnson, M.; Bodi, A.; Schulz, L.; Gerber, T. Vacuum Ultraviolet Beamline at the Swiss Light Source for Chemical Dynamics Studies. *Nucl. Instrum. Meth. B.* **2009,** *610*, 597-603.

(25)   Bodi, A.; Sztaray, B.; Baer, T.; Johnson, M.; Gerber, T. Data Acquisition Schemes for Continuous Two-Particle Time-of-Flight Coincidence Experiments. *Revi. Sci. Instrum.* **2007,** *78*, 084102.

(26)   Sztàray, B.; Baer, T. Supression of Hot Electron in Treshold Photoelectron Photoion Coincidence Studies using Velocity Focussing Optics. *Rev. Sci. Instrum.* **2003,** *74*, 3763.

(27)   Scheer, A. M.; Mukarakate, C.; Robichaud, D. J.; Nimlos, M. R.; Ellison, G. B. Thermal Decomposition Mechanisms of the Methoxyphenols: Formation of Phenol, Cyclopentadienone, Vinylacetylene, and Acetylene. *J. Phys. Chem. A* **2011,** *115*, 13381-13389.

(28)   Frisch, M. J.; Trucks, G. W.; Schlegel, H. B.; Scuseria, G. E.; Robb, M. A.; Cheeseman, J. R.; Scalmani, G.; Barone, V.; Mennucci, B.; Petersson, G. A., et al. Gaussian 09, Revision B.01. Wallingford CT, 2009.

(29)   Mozhayskiy, A.; Krylov, A. I. *ezSpectrum* http://iopenshell.usc.edu/downloads.

(30)   Curtiss, L. A.; Redfern, P. C.; Raghavachari, K. Gaussian-4 Theory. *J. Chem. Phys.* **2007,** *126*.

(31)   Montgomery, J. A.; Frisch, M. J.; Ochterski, J. W.; Petersson, G. A. A Complete Basis Set Model Chemistry. VI. Use of Density Functional Geometries and Frequencies. *J. Chem. Phys.* **1999,** *110*, 2822-2827.

(32)   Montgomery, J. A.; Frisch, M. J.; Ochterski, J. W.; Petersson, G. A. A Complete Basis Set Model Chemistry. VII. Use of the Minimum Population Localization Method. *J. Chem. Phys.* **2000,** *112*, 6532-6542.

(33)   Kreile, J.; Münzel, N.; Schulz, R.; Schweig, A. UV Photoelectron Spectrum of o-Xylylene — Detection of a Low-Energy Non-Koopmans (Shake-up) Ionization. *Chem. Phys. Lett.* **1984,** *108*, 609-612.

(34)   Rabalais, J. W.; Colton, R. J. Electronic Interaction between the Phenyl Group and its Unsaturated Substituents. *J. Electron Spectrosc.* **1972,** *1*, 83-99.

(35)   Kesper, K.; Münzel, N.; Pietzuch, W.; Specht, H.; Schweig, A. Matrix Isolation Radiation Chemistry and Photochemistry: Electronic Absorption Spectra of o-Xylylene and Benzocyclobutene Radical Cations; Localization of Koopmans and Non-Koopmans Bands in the Photoelectron Spectra of o-Xylylene, Styrene, Toluene, o-Xylene and Benzocyclobutene. *J. Mol. Struct.: THEOCHEM* **1989,** *200*, 375-400.

(36)   Dyke, J. M.; Ozeki, H.; Takahashi, M.; Cockett, M. C. R.; Kimura, K. A Study of Phenylacetylene and Styrene, and their Argon Complexes PA--Ar and ST--Ar with Laser Threshold Photoelectron Spectroscopy. *J. Chem. Phys.* **1992,** *97*, 8926-8933.

(37)   Koenig, T.; Wielesek, R.; Snell, W.; Balle, T. Helium(I) Photoelectron Spectrum of p-Quinodimethane. *Journal of the American Chemical Society* **1975,** *97*, 3225-3226.

(38)   Kwon, C. H.; Kim, H. L.; Kim, M. S. Vibrational Analysis of Vacuum Ultraviolet Mass-Analyzed Threshold Ionization Spectra of Phenylacetylene and Benzonitrile. *J. Phys. Chem. A* **2003,** *107*, 10969-10975.

(39)   Pugliesi, I.; Tonge, N. M.; Hornsby, K. E.; Cockett, M. C. R.; Watkins, M. J. An Examination of Structural Characteristics of Phenylacetylene by Vibronic and Rovibronic Simulations of ab Initio Data. *Phys. Chem. Chem. Phys.* **2007,** *9*, 5436-5445.

(40)   Emdee, J. L.; Brezinsky, K.; Glassman, I. Oxidation of O-xylene. *Symp. (Int.) Comb.* **1991,** *23*, 77-84.

(41)   Emdee, J. L.; Brezinsky, K.; Glassman, I. High-Temperature Oxidation Mechanisms of m- and p-Xylene. *J. Phys. Chem.* **1991,** *95*, 1626-1635.

(42)   Grela, M. A.; Amorebieta, V. T.; Colussi, A. J. Pyrolysis of Styrene: Kinetics and Mechanism of the Equilibrium Styrene .tautm. Benzene + Acetylene. *J. Phys. Chem.* **1992,** *96*, 9861-9865.

(43)   Zou, S.; Bowman, J. M. A New ab Initio Potential Energy Surface describing Acetylene/Vinylidene Isomerization. *Chem. Phys. Lett.* **2003,** *368*, 421-424.

(44)   Mueller-Markgraf, W.; Troe, J. Thermal Decomposition of Ethylbenzene, Styrene, and Bromophenylethane: UV Absorption Study in Shock Waves. *J. Phys. Chem.* **1988,** *92*, 4914-4922.

(45)   Dorrestijn, E.; Pugin, R.; Ciriano Nogales, M. V.; Mulder, P. Thermal Decomposition of chroman: Reactivity of *o*-Quinone Methide. *J. Org. Chem.* **1997**, *62*, 4804.

(46)   da Silva, G.; Bozzelli, J. W. Quantum Chemical Study of the Thermal Decomposition of *o*-Quinone Methide (6-methylene-2,4-cyclohexadien-1-one). *J. Phys. Chem. A* **2007**, *111*, 7987-7994.

(47)   Bland, J.; da Silva, G. A Detailed Chemical Kinetic Model for Pyrolysis of the Lignin Model Compound Chroman. *AIMS Environ. Sci.* **2013**, *1*, 12-25.

(48)   da Silva, G.; Trevitt, A. J.; Steinbauer, M.; Hemberger, P. Pyrolysis of Fulvenallene (C_7H_6) and Fulvenallenyl (C_7H_5): Theoretical Kinetics and Experimental Product Detection. *Chem. Phys. Lett.* **2011,** *517*, 144-148.

(49)   Friedrichs, G.; Goos, E.; Gripp, J.; Nicken, H.; Schonborn, J.-B.; Vogel, H.; Temps, F. *Z. Phys. Chem.* **2009**, *223*, 387.

(50)   Hammad, L. A.; Wenthold, P. G. Synthesis, Characterization, and Reactivity of the m-Xylylene Anion in the Gas Phase. The Enthalpy of Formation of m-Xylylene. *J. Am. Chem. Soc.* **2000,** *122*, 11203-11211.

(51)   Neuhaus, P.; Grote, D.; Sander, W. Matrix Isolation, Spectroscopic Characterization, and Photoisomerization of m-Xylylene. *J. Amer. Chem. Soc.* **2008,** *130*, 2993-3000.

(52)   Wenthold, P. G.; Kim, J. B.; Lineberger, W. C. Photoelectron Spectroscopy of m-Xylylene Anion. *J. Amer. Chem. Soc.* **1997,** *119*, 1354-1359.

(53)   Ozkan, I.; Kinal, A. Competing Pathways in the [2 + 2] Cycloadditions of Cyclopentyne and Benzyne. A DFT and ab Initio Study. *J. Org. Chem.* **2004,** *69*, 5390-5394.

(54)   Cool, T. A.; Wang, J.; Nakajima, K.; Taatjes, C. A.; McLlroy, A. Photoionization Cross Sections for Reaction Intermediates in Hydrocarbon Combustion. *Int. J. Mass Spectrom.* **2005,** *247*, 18-27.

(55)   Savee, J. D.; Soorkia, S.; Welz, O.; Selby, T. M.; Taatjes, C. A.; Osborn, D. L. Absolute Photoionization Cross-Section of the Propargyl Radical. *J. Chem. Phy.s* **2012,** *136*, 134307.

(56)   Zhang, X.; Chen, P. Photoelectron Spectrum of o-Benzyne. Ionization Potentials as a measure of Singlet-Triplet Gaps. *J. Am. Chem. Soc.* **1992,** *114*, 3147-3148.

Table of Contents – Graphic